ARTICLE   **OPEN**

Check for updates

Arctic amplification, and its seasonal migration, over a wide range of abrupt CO_2 forcing

Yu-Chiao Liang [1,2 ✉], Lorenzo M. Polvani [1,3,4] and Ivan Mitevski[4]

Arctic amplification (AA), the larger warming of the Arctic compared to the rest of the planet, is widely attributed to the increasing concentrations of atmospheric CO_2, and is caused by local and non-local mechanisms. In this study, we examine AA, and its seasonal cycle, in a sequence of abrupt CO_2 forcing experiments, spanning from 1 to 8 times pre-industrial CO_2 levels, using a state-of-the-art global climate model. We find that increasing CO_2 concentrations give rise to stronger Arctic warming but weaker AA, owing to relatively weaker warming of the Arctic in comparison with the rest of the globe due to weaker sea-ice loss and atmosphere-ocean heat fluxes at higher CO_2 levels. We further find that the seasonal peak in AA shifts gradually from November to January as CO_2 increases. Finally, we show that this seasonal shift in AA emerges in the 21st century in high-CO_2 emission scenario simulations. During the early-to-middle 21st century AA peaks in November–December but the peak shifts to December-January at the end of the century. Our findings highlight the role of CO_2 forcing in affecting the seasonal evolution of amplified Arctic warming, which carries important ecological and socio-economic implications.

INTRODUCTION

Arctic amplification (AA), the simple fact that the Arctic surface warms at a faster rate than the rest of the globe[1,2], is the most prominent feature of increasing atmospheric concentrations of greenhouse gases (GHG)[3–5], as a consequence of anthropogenic emissions. Within the Arctic, AA has had wide impacts on ecosystems and socio-economic activities[5]. For example, amplified Arctic warming has melted sea ice in shelf regions, and opened a new route for polar commercial shipping[6–8], fishery activities[9,10], and natural resource extractions[11]. AA has also been suggested to exert a far-reaching influence on extreme weather events in North America, Europe, and Northern Siberia[12–15], although this influence—and the possible dynamical pathways—are poorly understood and, in fact, remain vigorously debated[16–21]. Improving our understanding of AA and its causes is, therefore, not only of scientific merit, but also has regional and, potentially, global implications[5].

Simulations with general circulation models (GCM) forced by increasing CO_2 concentrations had revealed that AA is not a consequence of a larger radiative CO_2 forcing at the poles than at lower-latitudes, as one might have naively imagined: in fact, upon increasing CO_2 concentrations, the direct radiative forcing is larger at the equator than at the poles[22,23]. AA, is thus produced by local positive feedbacks[22,24–28], poleward heat and moisture transports[28–33], oceanic heat exchange mechanisms[34–36], and, possibly, complex interactions among these factors[37,38]. While the seasonal evolution of AA is a complex phenomenon, involving multiple coupled mechanisms with different seasonal features[35,38–40], it is widely accepted that the sea-ice conditions—and the accompanying atmosphere-ocean heat exchange—are an important player[35,36,41–51]. The amplified Arctic warming, ultimately caused by GHG increases, is thus closely tied to the seasonal evolution of sea ice. During Northern Hemisphere summer, sea-ice reduction allows absorbed solar radiation to warm the ocean mixed layer, a

process enhanced by the sea-ice albedo feedback[2,39,52–54]. Then, in the following autumn and winter, when the atmosphere rapidly cools, the enhanced air-sea thermal contrast results in stronger surface heat and moisture fluxes entering the atmosphere, and these produce stronger lower-tropospheric warming, enhanced by the sea-ice insulation effect[50,55] and longwave feedback processes[22,38,56]. Fully-coupled ocean-atmosphere-sea-ice-land GCM experiments in which Arctic sea-ice loss is artificially specified showed a clear causal link between sea-ice loss and amplified Arctic atmospheric warming[44–48,57,58]. More importantly, since the amount of future Arctic sea-ice loss depends on the seasonal evolution of sea ice as the climate warms[59,60], one would expect the seasonal cycle of AA to correspondingly evolve with increasing CO_2 as a recent study revealed[61]. This is one of the key motivations for this work: to investigate the seasonal cycle of AA in response to CO_2 forcing.

In addition, to date, most modeling studies of Arctic climate change are based on the experiments with doubling (hereafter 2×) or, at most, quadrupling (hereafter 4×) of CO_2 concentrations from pre-industrial levels (~285 ppm, hereafter PI)[22,38,62]. Because the Arctic climate system is characterized by large internal variability[63–66], exploring larger CO_2 values would be useful to obtain a better signal-to-noise ratio. Moreover, in practical terms, looking at higher CO_2 values is of interest because in the high emission scenario used for climate projections by Phase 6 of the Coupled Model Intercomparison Project (CMIP6), CO_2 levels can reach higher values than $4 \times CO_2$ after the year 2100[67]. However, scenario integrations involve many forcings that change in complex ways, often non-monotonically (e.g., aerosols or ozone-depleting GHGs), thus complicating our understanding of the Arctic response to increasing CO_2.

In order to clearly bring out the characteristics of sea-ice loss and AA at high CO_2 concentrations, we here analyze a set of GCM simulations performed in a recent study[68], with abrupt forcing

[1]Lamont-Doherty Earth Observatory, Columbia University, Palisades, NY, USA. [2]Department of Atmospheric Sciences, National Taiwan University, Taipei, Taiwan. [3]Department of Earth and Environmental Sciences, Columbia University, New York, NY, USA. [4]Department of Applied Physics and Applied Mathematics, Columbia University, New York, NY, USA. ✉email: yuchiaoliang@ntu.edu.tw

spanning the range $1 \times$ to $8 \times CO_2$. This allows us to document the response of the Arctic climate system as a function of CO_2 over a broad range of values, without the confounding interference of other forcings. Having documented that response, we explicitly demonstrate that the results obtained from the abrupt $n \times CO_2$ simulations are not of merely academic interest. Analyzing the Arctic climate evolution under high-CO_2 emissions scenarios, in both single-model large-ensembles and CMIP6 multi-model ensemble, we show that the key features of the response seen in the abrupt CO_2-only forcing simulations also emerge in the realistic scenario simulations throughout the course of 21st century.

RESULTS

Arctic warming in response to abrupt CO_2 forcing

We start by examining the response of the annual-mean Arctic surface air temperature (SAT) to CO_2 forcing in the fully coupled ocean-atmosphere-sea-ice-land model experiments. In this study, we define the response as the difference, averaged over the last 30 years of the simulations, between the $n \times CO_2$ and the $1 \times CO_2$ (i.e., the pre-industrial) experiments, with n ranging from 2 to 8. Figure 1a shows that, in fully coupled model experiments, the Arctic SAT response becomes stronger as CO_2 forcing increases (solid line with circle symbols) with range from 6.3 K for $2 \times CO_2$ to 17.1 K for $8 \times CO_2$. As the Arctic SAT warming is coupled closely to sea-ice retreat[35,36,38], the corresponding sea-ice extent (SIE) response decreases with increasing CO_2 (Fig. 1b). The weaker SAT and SIE responses at $4 \times CO_2$ than at $3 \times CO_2$ are associated

with a substantial weakening of the Atlantic meridional overturning circulation (AMOC) in $4 \times CO_2$ experiment[68], which results in less oceanic heat transport into the Arctic, and reduced Arctic warming and sea-ice loss. We confirm this by examining the corresponding slab ocean model experiments, in which changes in ocean dynamics are absent. There are no kinks at $4 \times CO_2$ in slab ocean model SAT and SIE responses (dashed lines with triangles). It is important to note that the non-monotonic climate response at $4 \times CO_2$ is not confined within the Arctic, as it is present in many aspects of the climate response in the Northern Hemisphere (e.g., the AMOC, tropical expansion, precipitation), and has been shown not to be a model-dependent feature (see a recent study[68] using the same abrupt CO_2 experiments for more details).

Examining the $n \times CO_2$ simulations further, we find increasing surface turbulent (latent and sensible) heat fluxes entering the atmosphere as CO_2 increases (Fig. 1c), as one would expect from the larger areas of open water accompanying the larger sea-ice losses. The consistent responses of SAT, SIE, and air-sea heat fluxes confirm that these components are closely coupled with each other, and they are likely working together to enhance the warming of the lower-troposphere, as recent studies have argued[35,36,38]. We also examine the response of the surface shortwave and longwave radiative fluxes (positive upward into the atmosphere), both of which show more negative values at greater CO_2 forcing (Supplementary Fig. 1), indicating that they penetrate more into the ocean and leave the atmosphere cooler as CO_2 increases. We interpret the shortwave and longwave radiative changes to be both a cause and a consequence of the warmer troposphere and larger sea-ice retreat. The reader is likely well aware that, while we have only presented the annual-mean responses, both turbulent heat and radiative fluxes have
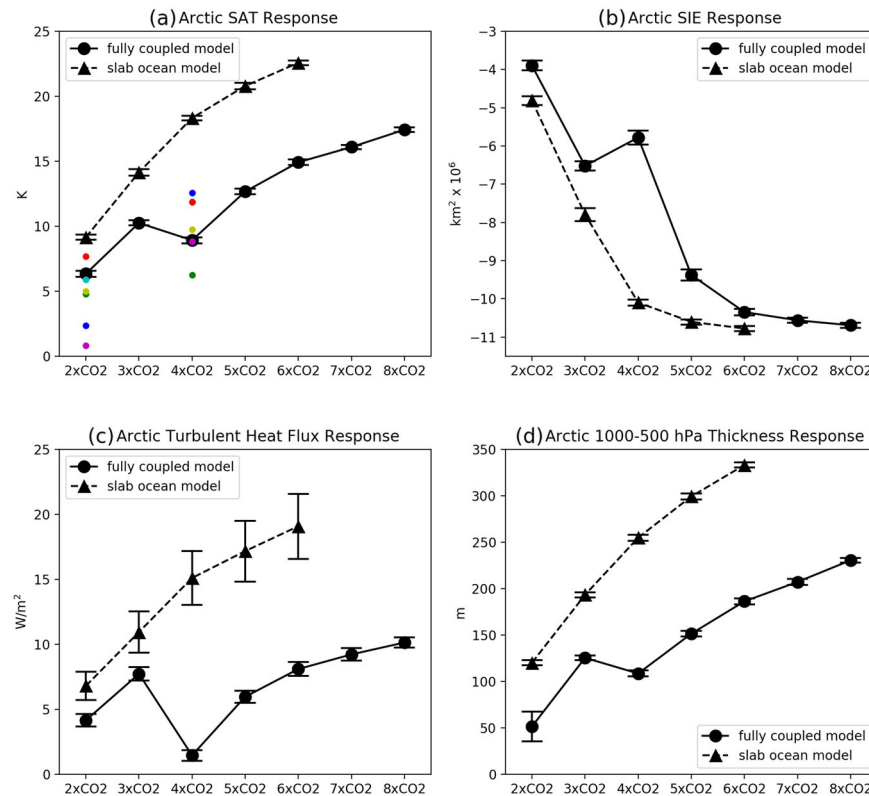

Fig. 1 Annual-mean Arctic surface and tropospheric response as a function of CO_2 forcing in fully coupled and slab ocean model experiments. a Surface air temperature (SAT) response. The colored dots are the 2× and $4 \times CO_2$ experiments from six CMIP6 models: CESM2 (blue), CNRM-CM6-1 (cyan), GISS-E2-1-G (green), MIROC6 (yellow), MRI-ESM2-0 (magenta), TaiESM1 (red). **b** Sea-ice extent (SIE) response. **c** Turbulent heat flux (latent plus sensible heat components) response (positive value means heat fluxes from ocean to atmosphere). **d** 1000–500 hPa thickness (geopotential height difference between 1000 hPa and 500 hPa) response. The solid line with circle symbols represents responses for the fully coupled model experiments, whereas the dashed line with triangle symbols for the slab ocean model experiments. Error bars denote 95% confidence intervals calculated using Student's t-distribution.
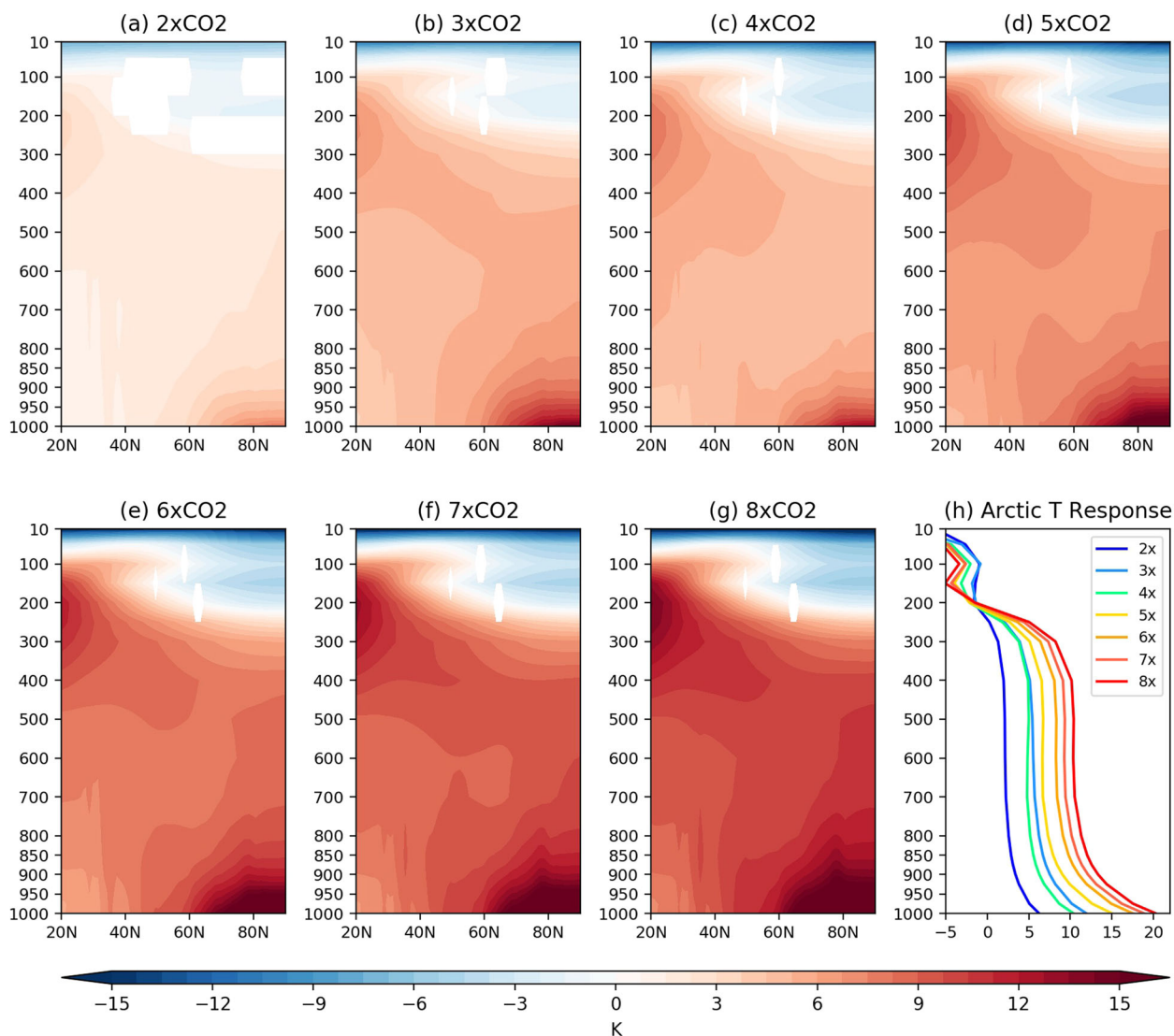
Fig. 2 Vertical structure of the zonal-mean air temperature response to increasing CO₂ forcing. a–g The zonal-mean air temperature responses for 2× to 8 × CO₂ respectively in fully coupled model experiments. Only the responses passing Student's *t*-test with 95% confidence interval are shown. **h** Polar cap-averaged (60°N–90°N) air temperature responses.

strong seasonal cycles[35,36,39], but we postpone the discussion of the seasonal features of the responses to the next section in order to first examine the vertical structure.

As seen in Fig. 2a–g, our simulations reveal that the vertical extent of the zonal-mean air temperature response not only becomes stronger but also penetrates deeper into the troposphere as the forcing is increased. The Arctic warming response of $2 \times CO_2$ is rather shallow, mostly below 850 hPa, but reaches much higher as the forcing is increased to $8 \times CO_2$. Quantitatively, the polar cap-averaged (60°N–90°) temperature responses are about 6 K at 1000 hPa and 3 K at 500 hPa for $2 \times CO_2$, whereas they are about 20 K at 1000 hPa and 12 K at 500 hPa for $8 \times CO_2$ (Fig. 2h). These vertical profiles manifest a stronger bottom-heavy warming structure and a larger vertical temperature gradient at higher CO₂: this favors the lapse-rate feedback which enhances the near-surface Arctic warming, as many studies highlighted[22,24,28,38]. Similar results are found in slab ocean model experiments (Supplementary Fig. 2), and the overall stronger warming responses appear consistent with previous studies[69,70]. As to whether the amplified Arctic warming might be able to impact mid-latitude weather and climate, it has been suggested that Arctic warming extending into the middle

troposphere (e.g., 500 hPa) would affect the mid-latitude circulation[71–73] and possibly cause cooling in mid-latitudes[72]. We have calculated the 1000–500 hPa thickness over the polar cap for all the $n \times CO_2$ simulations and find that the troposphere indeed becomes thicker as CO₂ increases (Fig. 1d), and this may lead to mid-latitude cooling, although this signal could be masked by the prevailing global warming.

Arctic amplification and its seasonal cycle in response to CO₂ forcing

We now turn from Arctic warming to Arctic amplification (AA), which we here quantify with a non-dimensional factor (hereafter AAF) defined as the Arctic-averaged (60°N–90°N) SAT response divided by a globally-average one. Although both the annual Arctic and the global SAT increase rapidly in the first 20-year simulations, in the $n \times CO_2$ runs the annual-mean AAF (Fig. 3a) decreases for the first 70 years and then flattens out, with AAF values around 2 for the higher CO₂ forcings (5× to $8 \times CO_2$), but somewhat larger for 2× and $3 \times CO_2$. The $4 \times CO_2$ case shows the smallest AAF, and deviates from other cases because of the weaker Arctic warming response (Fig. 1a) related to the AMOC
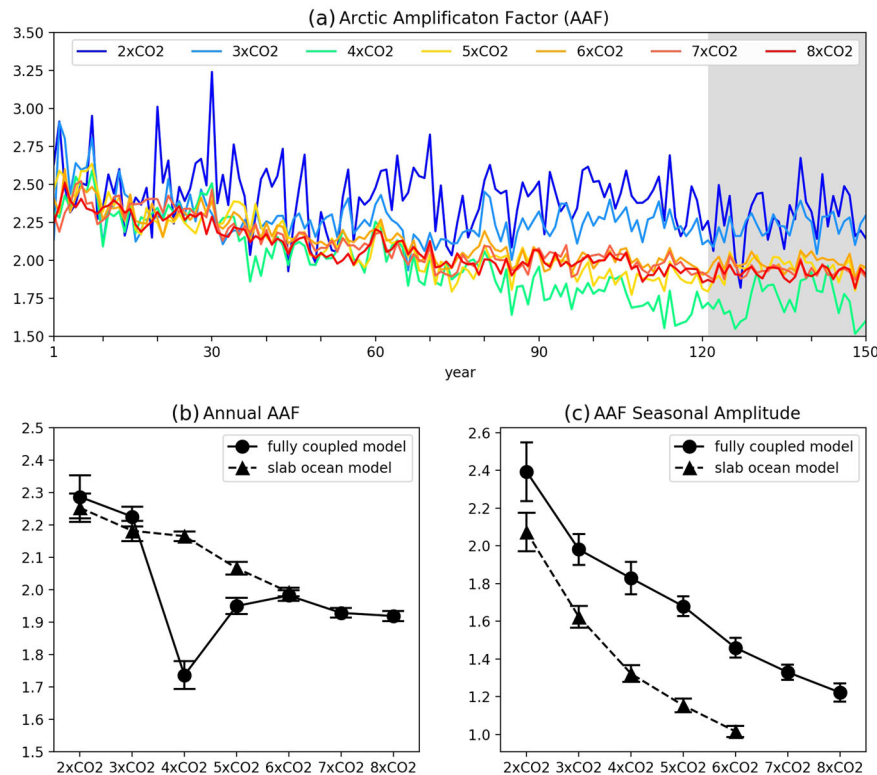
Fig. 3 Time evolution and annual-mean amplitude of the AAF in the abrupt CO_2 forcing experiments. a The evolution of the annual AAF for $2\times$ to $8\times CO_2$ in fully coupled model experiments. The last 30-year period is shaded with grey. **b** Annual-mean AAFs as functions of CO_2 forcing. **c** The AAF annual amplitude or seasonal range, defined as the maximum AAF minus minimum AAF of the mean seasonal cycle response. In **b** and **c**, the solid line with circle symbols represents responses for the fully coupled model experiments, whereas the dashed line with triangle symbols for the slab ocean model experiments. Error bars denote 95% confidence intervals calculated using Student's *t*-distribution.

slowdown, as discussed in the previous section. Focusing on the last 30 years of each simulation (grey shading in Fig. 3a), we find that the AAF decreases from about 2.3 to 1.9 as the forcing is increased from $2\times$ to $8\times CO_2$ (solid line with circles in Fig. 3b). The AAFs in slab ocean model experiments show similar decreasing values, but without the $4\times CO_2$ drop (dashed line with triangles in Fig. 3b), confirming again that the ocean dynamics associated with the AMOC slowdown is the main cause of the AAF drop at $4\times CO_2$ value in the fully coupled model experiment. We also investigate the seasonal amplitude of AAF, defined as the maximum minus the minimum of 30-year means, and find that it decreases with increasing CO_2 (Fig. 3c). This indicates that smaller seasonal variations would occur at high CO_2 concentrations.

However, we would be missing out on an important aspect of the Arctic response to CO_2 forcing if we limit our discussion of the AAF to the annual mean. This is because the response of Arctic air temperatures, sea ice, and atmosphere-ocean heat exchange (and the associated feedback mechanisms) depends strongly on season[35,39]. For example, over the period 1958–2017, the warming of the Arctic in boreal winter (about 4 K) has been five times larger than in summer (about 0.8 K), based on a reanalysis data (and GCM simulations), as shown in Fig. 1 of a recent study[35]. We thus next examine, in some details, the seasonal evolution of the Arctic response to increasing CO_2, starting with the AAF.

The seasonal cycle of AAF at increasing CO_2 concentrations, averaged over the last 30-year of the abrupt forcing simulations, is shown in Fig. 4b. Two features immediately stand out: (1) the AAF decreases at larger CO_2 forcing, and (2) the month of the largest AAF shifts to a later winter season. Investigation into the seasonal evolution of AAF from July to June indicates that the AAF maximum values, decreasing with CO_2 forcing, determine the

decrease in annual amplitude, because the minimum values do not respond much (Fig. 4b). We further find that the AAF peak occurs in November for $2\times CO_2$ case, and the peak progresses to December for $3\times$ to $5\times CO_2$, and then to January for yet higher CO_2 concentrations. This shift is dominated by the seasonal evolution of Arctic SAT response (Fig. 4a), not the extra-Arctic SAT response (Fig. 4d), referenced to the month of July (i.e., with the month of July value subtracted out). On the other hand, the global SAT seasonal responses are largely controlled by Arctic ones (c.f., 4c and 4a). We also find similar seasonal shifts of the peak AAF from November to December and the dominant roles of Arctic SAT responses in the AAF in slab ocean model experiments (Supplementary Figs. 3a, b). Our results suggest that the AA is delayed by 1 to 2 months in response to stronger CO_2 forcing.

To investigate the underlying mechanism, which we expect is closely related to the sea-ice conditions and atmosphere-ocean heat fluxes in the cold season, we perform the same seasonal cycle analysis for Arctic SIE and turbulent (latent plus sensible) heat fluxes (Fig. 4e and f, respectively). It is evident that the largest SIE loss occurs in most runs (2 to $5\times CO_2$) about one month before the turbulent heat flux maximum (which shift from November to December) in fully coupled model experiments, indicating that the sea-ice loss tends to produce the atmosphere-ocean heat fluxes and eventually give rise to AAF shifts. At higher CO_2 forcing (7 and $8\times CO_2$), the largest SIE loss occurs almost together with the turbulent heat flux maximum, suggesting that this mechanism contracts with time. On the other hand, the net surface shortwave fluxes are nearly zero in boreal winter, and thus are unlikely to play an important role (Supplementary Figs. 4a and b). The net surface longwave fluxes do show seasonal shifts during the cold season, but overall they are lagged by about one month in fully coupled
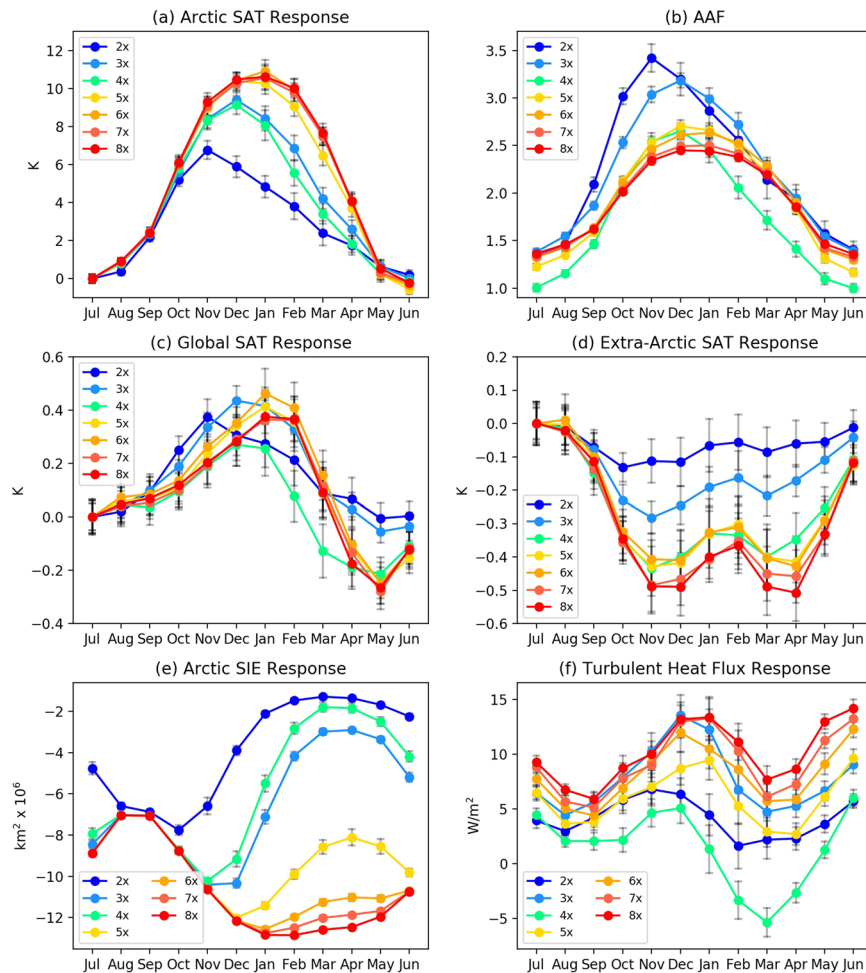
Fig. 4 Seasonal evolutions of the Arctic SAT, SIE, turbulent heat flux response, and AAFs in the abrupt CO_2 forcing experiments. a The evolution of Arctic SAT responses for 2× to 8 × CO_2. **b** Similar as (**a**) but for AAF. **c**, **d** Same as (**a**) but for global and extra-Arctic (90°S–59°N) SAT responses. **e**, **f** Same as (**a**) but for SIE and turbulent heat flux responses. Error bars denote 95% confidence intervals calculated using Student's t-distribution. Values in **a**, **c** and **d** are referenced to July values. All quantities are computed from the fully-coupled model runs.

model experiments (Supplementary Fig. 4b) compared to the shifts in SAT, SIE, and turbulent heat fluxes; this leads us to conclude that they are unlikely to be a driver of the seasonal shift, and are more likely a consequence, as revealed in the annual-mean values. In the slab ocean model experiments, the longwave fluxes do not show consistent seasonal shifts in 4× to 6 × CO_2 cases (Supplementary Fig. 4d), reflecting the lack of interactive ocean dynamics in regulating the climatological seasonal cycle. Further analysis would be needed to clarify the longwave flux differences between fully coupled and slab ocean model experiments. Taken in combination, these results suggest that the shift of the AAF peak from November to December and January, in response to increasing CO_2 forcing, is mainly governed by the interactive processes involving SAT, SIE, and atmosphere-ocean heat flux components.

The above analysis could be misleading because the proposed mechanism is supposed to only work above the Arctic ocean, not the Arctic land. To address this issue, we perform the same analysis but with the ocean-only and land-only Arctic domains. Supplementary Figure 5 shows the ocean-only Arctic SAT response, AAF, and turbulent heat flux response: these are similar, though slightly weaker, to the results in Fig. 4. In contrast, the land-only counterparts do not show consistent seasonal shifts (Supplementary Fig. 6). We further separate the ocean-only Arctic domain into ice-free and ice-covered regions, and find that the seasonal shift only occurs in the latter. These additional analyses

not only confirm that the dominant role of the coupling between SAT, SIE, and atmosphere-ocean heat flux in shifting the AAF, but also suggest that the land component does not contribute much to the shift.

Because the above analyses are based on very simple abrupt $n \times CO_2$ forcing experiments, they provide a very clean benchmark for quantifying the seasonal shift of the AAF with increasing CO_2. However, one might wonder whether they are too idealized to be of practical value. To address this concern, we finally turn our attention to more realistic scenarios, as those would be more informative for stakeholders and policymakers. We thus analyze a set of single-model initial-condition large ensembles (SMILEs) from Multi-Model Large Ensemble Archive (MMLEA)[74]. All the SMILEs simulations considered here were forced with GHG emissions and other forcings following the Representative Concentration Pathway 8.5 (RCP85) after the year 2005. The goal of this exercise is to determine whether the AAF also shifts in the scenarios, and if so when.

We first examine the Community Earth System Model version 1 (CESM1)[75] SMILE, which was produced with the exact same model configuration used in our fully coupled abrupt $n \times CO_2$ forcing experiments, to investigate the AA peak shift from early to late 21st century. Figure 5a and b show the Arctic SAT responses and AAFs (referenced to 1921–1950 mean) averaged over periods 2011–2040, 2041–2070, 2071–2100 periods. The peaks of the SAT response and of the AAF show consistent shifts from November to
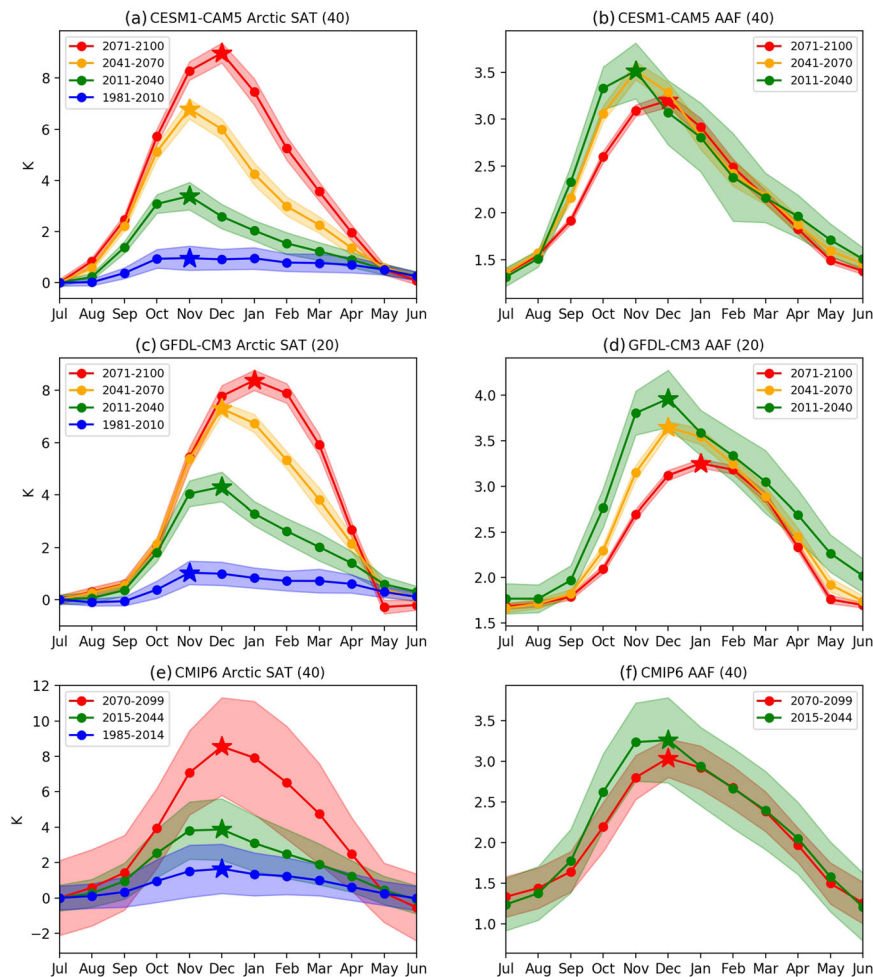
Fig. 5 Seasonal evolutions of the Arctic SAT responses and AAF in the CESM1 and GFDL-CM3 SMILEs, and the CMIP6 models. a The evolution of Arctic SAT responses (reference to 1921–1950 averages) in CESM1 SMILE. **b** Similar as (**a**) but for AAF. **c**, **d** Similar as (**a**), (**b**) but for GFDL-CM3 SMILE. **e**, **f** Similar as (**a**), (**b**) but for multi-model mean of 40 CMIP6 models. In **a**–**d**, the solid line represents ensemble means and the color shading indicates one standard deviation across ensemble members. In **e**, **f**, the solid line represents multi-model means and the color shading indicates one standard deviation across models. In **a**, **c**, **e**, all values are referenced to July values. The ensemble or model size is labeled in the parenthesis of each title.

December, with the AAF maximum decreasing from about 3.5 to 3.2, as the 30-year periods approach the end of this century. This behavior is robust, as it can also be seen in the GFDL-CM3 SMILE, which also shows seasonal shifts of Arctic warming response and AAF (Fig. 5c, d). We also find that the CanESM2 shows a clear shift from November to December, and that the MPI-ESM also shows a shift (with larger January than November values for the 2071–2100 period, and smaller January than November values for other periods (see Supplementary Fig. 7).

Finally, we have examined the seasonal cycle of the SAT and the AAF in 40 different CMIP6 models (one member for each model) under the Shared Socioeconomic Pathway 5-8.5 (SSP585) scenario; the multi-model mean and cross-model spread are shown in Fig. 5e, f. While the seasonal shift of the AAF peak is not as marked as in our abrupt $n \times CO_2$ forcing experiments, or in the SMILEs, due to a relatively large inter-model spread, already identified in CMIP5 studies via local energy loss above sea-ice retreat regions[39], a shifting tendency of the peak from the earlier to the later decades is still present. The CMIP6 models under SSP585 forcing, therefore, exhibit the shifting tendency as the January value is larger than the November one in the late 21st century but not the case for other periods, and suggest that the seasonal shift in AA is very likely to emerge in the upcoming decades, with its precise timing depending on the amount of CO_2 concentrations in the

atmosphere (and being subject, of course, to model uncertainty). We have also examined the seasonal shift of the Arctic SAT response in each CMIP6 model (Supplementary Fig. 8): more than half of them show a 1- or 2-month shift, and the rest show at least some shifting tendency. Only one model shows reverse shifting (GISS-E2-1-G).

DISCUSSION

We have documented the warming of the Arctic in response to increasing concentrations of CO_2, from 2× to 8× its PI value, analyzing a suite of abrupt CO_2 forcing experiments from a recent study[68]. The annual-mean Arctic warming response is found to be closely coupled to the response of sea ice and surface turbulent heat fluxes, and become intensified at high CO_2 forcing due to more open water as a result of more sea-ice loss (and resultant sea-ice insulation effect[50,55]) and stronger heat fluxes entering the atmosphere in a nearly ice-free state. The vertical profile of the Arctic warming response is also found to extend higher into the troposphere as CO_2 increases, and thus may be able to produce a clearer Arctic warm-mid-latitude cold linkage, as suggested by a recent study[72]; however, the question of whether this may be overwhelmed by the overall CO_2-induced warming signal in mid-latitudes remains open. The annual AAF, on the other hand, is found to decrease as CO_2 forcing

increases, consistent with previous studies[35,52,55]. This weakening is mainly attributed to the relatively smaller sea-ice loss and the accompanying weaker turbulent heat fluxes at higher CO_2 levels compared to those at low CO_2 levels, which limits the degree of Arctic warming.

Our analysis of the seasonal evolution of Arctic climate in response to abrupt CO_2 forcing has yielded several new insights. The seasonal evolution of AAF shows that the peak value occurs in the cold season and shifts from November to December and January as CO_2 forcing increases. This seasonal AAF shift in our abrupt $n \times CO_2$ experiments stems from the shift of the Arctic SAT response, not the extra-Arctic SAT response, because no clear seasonal shift is seen outside the Arctic. These findings are also seen in the SMILEs and the CMIP6 models under high-CO_2 emission scenario: in those models, the shift of the AAF peak from November to December is projected to emerge in the second half of the 21st century, when CO_2 concentrations reach sufficiently high values. If the CO_2 emission continues to increase beyond the year 2100[67], the models project that the AAF peak will progress into January or February. Our findings have substantial implications for Arctic ecosystems and socio-economics. For instance, the timing of new commercial shipping routes[6–8] and fishery activities in the Arctic[9,10] in boreal winter may need to be re-assessed in upcoming decades if the projection from SMILEs and CMIP6 model we have analyzed proves to be realistic.

The ensemble spread in SMILE simulations represents the effect of internal variability, whereas the spread in the CMIP6 simulations also includes the structural model uncertainties[76,77]. It is clear from Fig. 5 that the former changes little as time progresses, whereas the latter increases substantially. This means that the structural model uncertainties may become important toward the end of the 21st century, as noted in a recent study[76] which also pointed out the increasing importance of scenario uncertainty (see also a recent study[78]). Therefore, caution is needed in interpreting the multi-model means in future projections, as the forced responses can be masked by structural and scenario uncertainties: this is likely the cause for the less apparent seasonal shift of the AAF peaks in CMIP6 multi-model mean. Our results have the additional value of examining single-model simulations with large-ensemble members, which shows the clear emergence of the delayed AAF peaks by the end of 21st century.

We propose that the dominant mechanism behind the shift of the seasonal AAF peak in Northern Hemisphere winter with increasing CO_2 involves the concomitant seasonal evolution of Arctic near-surface warming, sea-ice loss, and atmosphere-ocean heat exchange. Indeed, the close relationship between those three components, and their interactions, have been emphasized as the principal mechanism for cold-season amplified Arctic warming by many previous studies[35,39,49,54]. The lapse-rate and convective cloud feedbacks have also been highlighted by some previous studies as important in producing an amplified Arctic warming in winter[22,27]; however, more recent studies have demonstrated that they are either linked to ocean-to-atmosphere heat and moisture fluxes[35,37,38,40] or controlled by preceding sea-ice albedo feedback[36]. The water vapor feedback, on the other hand, is strong primarily during the sea-ice melting season[22,27,39]. In addition, the potential role of remote impacts from atmospheric and oceanic heat transports are yet to be investigated, although some studies have argued that their effects on near-surface Arctic warming are relatively small (due to the cancellation of dry and wet components)[22,39,42,53]. The above mechanisms are less likely, we believe, to play a dominant role in shifting the AAF peak in boreal winter as CO_2 increases, as supported by our analysis on the surface net shortwave and longwave fluxes. Nevertheless, we plan to perform a complete feedback decomposition analysis[35,38,79] in a future study, to further clarify their contributions and quantify their uncertainties. In addition, the sea-ice heat capacity mechanism has also been proposed as an important player in the seasonal shift of Arctic temperature change[80]. Finally, the CO_2 forcing structure has also been suggested to be critical for the amplified Arctic warming[28,81], and we also hope to investigate that in the future.

METHODS

Fully coupled and slab ocean model abrupt CO_2 forcing experiments

In this study, we analyze a set of abrupt CO_2 fully coupled and slab ocean model experiments, carried out in a recent study[68]. In the fully coupled model experiments, the Community Earth System Model version 1 (CESM1), consisting of the Community Atmosphere Model version 5 (CAM5, 30 vertical levels) and parallel ocean program version 2 (POP2, 60 vertical levels) with nominal 1° horizontal resolution in all model components[75], was forced by 1× (i.e., PI CO_2), 2×, 3×, 4×, 5×, 6×, 7×, and 8× CO_2 forcings, while all other trace gases, ozone concentrations, and aerosols were fixed at PI values. Following the 4× CO_2 protocol for CMIP6, all of our fully coupled model experiments are integrated for 150 years starting from PI initial conditions. The slab ocean model experiments use the same atmospheric component which is, however, coupled to a mixed-layer ocean with prescribed ocean heat transport[82], and kept constant at PI annual and monthly values derived from CESM1 simulations, respectively. We also show the results of 60-year slab ocean model experiments with 1×, 2×, 3×, 4×, 5×, and 6× CO_2 forcings. In these runs, we define the response in any variable of interest as the difference between any of the $n \times CO_2$ runs and the 1× CO_2 run (i.e., the PI control run), averaged over the last 30 years of each integration. We have verified that our results are not sensitive to the choice of averaging period.

SMILE model output

We analyze monthly SAT data from six SMILEs in the Multi-Model Large Ensemble Archive (MMLEA)[74]. These SMILEs model runs were forced with historical and RCP8.5 emission scenarios, and were performed under the CESM1 Large Ensemble Community Project[75] (40 members), the Canadian Earth System Model (CanESM2) Large Ensemble[83] (50 members), the Commonwealth Scientific and Industrial Research Organisation (CSIRO-Mk3.6.0) Large Ensemble[84] (30 members), Geophysical Fluid Dynamics Laboratory (GFDL-CM3) Large Ensemble[85] (20 members), the Geophysical Fluid Dynamics Laboratory Earth System Model (GFDL-ESM2M) Large Ensemble[86] (30 members), and the Max Planck Institute Earth System Model (MPI-ESM) Grand Ensemble[87] (100 members). We do not show results of GFDL-ESM2M and CSIRO-Mk3.6.0 because their sea-ice extents during the 21st century are unrealistically high[76] and, as a consequence, changes in the AAF are rather small. For CESM1, GFDL-CM3, and MPI-ESM, the SAT response is calculated as the SAT difference between the 30-year mean in the historical or RCP8.5 periods and 30-year mean in 1921–1950 period (which we take as the reference period). The CanESM2 runs only start at 1950, so we use 1951–1980 as the reference period.

CMIP6 output

Monthly SAT data from 40 Coupled Model Intercomparison Project phase 6 (CMIP6)[88] models are used in this study. All models are from the r1i1p1 ensemble with PI, historical and Shared Socioeconomic Pathway 5-8.5 (SSP585, an update of RCP8.5 forcing scenario) runs available. These models include: ACCESS-CM2, ACCESS-ESM1-5, AWI-CM-1-1-MR, BCC-CSM2-MR, CAMS-CSM1-0, CanESM5, CESM2, CESM2-WACCM, CIESM, CMCC-CM2-SR5, CNRM-CM6-1-HR, CNRM-CM6-1, CNRM-ESM2-1, E3SM-1-1, EC-Earth3, EC-Earth3-Veg, FGOALS-f3-L, FGOALS-g3, FIO-ESM-2-0, GFDL-CM4, GFDL-ESM4, GISS-E2-1-G, HadGEM3-GC31-LL, HadGEM3-GC31-MM, IITM-ESM, INM-CM4-8, INM-CM5-0, IPSL-CM6A-LR, KACE-1-0-G, MCM-UA-1-0, MIROC6, MIROC-ES2L, MPI-ESM1-2-HR, MPI-ESM1-2-LR, MRI-ESM2-0, NESM3, NorESM2-LM, NorESM2-MM, TaiESM1, UKESM1-0-LL. For each model, the SAT response is calculated as the SAT difference between the 30-year mean in historical or SSP585 runs and 30-year mean in PI runs. We then take an average of these SAT responses as multi-model mean SAT response shown in Fig. 5. Six models (i.e., CESM2, CNRM-CM6-1, GISS-E2-1-G, MIROC6, MRI-ESM2-0, and TaiESM1) having both 2× CO_2 and 4× CO_2 experiments are analyzed and presented in Fig. 1a.

Statistical significance analysis

Statistical significance is indicated with error bars in Figs. 1, 3, and 4, calculated using a Student's t-distribution with 95% confidence intervals using a Python statistical package (https://docs.scipy.org/doc/scipy/reference/generated/scipy.stats.t.html) that considers the probability density function $f(x, v) = \frac{\Gamma((v+1)/2)}{\sqrt{\pi v}\Gamma(v/2)}\left(1 + x^2/v\right)^{-(v+1)/2}$, where v is the degree of freedom and Γ is the gamma function. In Fig. 2, the statistical significance of 30-year mean differences is determined using a two-sided Student's t-test, the null hypothesis being that the difference of 30-year mean is zero. If the null hypothesis can be rejected with a 5% significance level (i.e., the p-value <0.05), we refer to the mean difference as statistically significant.

DATA AVAILABILITY

The fully coupled and slab ocean model abrupt CO_2 simulations are available upon request from the corresponding author. The SMILEs were obtained from MMLEA website (https://www.cesm.ucar.edu/projects/community-projects/MMLEA/), and CMIP6 results from World Climate Research Programme (https://www.wcrp-climate.org/wgcm-cmip/wgcm-cmip6).

CODE AVAILABILITY

Computer code used to generate results is available upon corresponding author's GitHub repository (https://github.com/yuchiaol/Arctic_warming_seasonality) or request from the corresponding author.

REFERENCES

1. Graversen, R. G., Mauritsen, T., Tjernström, M., Källén, E. & Svensson, G. Vertical structure of recent Arctic warming. *Nature* **451**, 53–56 (2008).
2. Serreze, M., Barrett, A., Stroeve, J., Kindig, D. & Holland, M. The emergence of surface-based Arctic amplification. *Cryosphere* **3**, 11–19 (2009).
3. Manabe, S. & Wetherald, R. T. The effects of doubling the CO_2 concentration on the climate of a general circulation model. *J. Atmos. Sci.* **32**, 3–15 (1975).
4. Stocker, T. et al. *Climate Change 2013: the Physical Science Basis: Working Group I Contribution to the Fifth Assessment Report of the Intergovernmental Panel on Climate Change* (Cambridge University Press, 2014).
5. Meredith, M. et al. in *IPCC Special Report on the Ocean and Cryosphere in a Changing Climate*, Ch. 3 (IPCC, 2019).
6. Smith, L. C. & Stephenson, S. R. New trans-Arctic shipping routes navigable by midcentury. *Proc. Natl Acad. Sci. USA* **110**, E1191–E1195 (2013).
7. Melia, N., Haines, K. & Hawkins, E. Sea ice decline and 21st century trans-Arctic shipping routes. *Geophys. Res. Lett.* **43**, 9720–9728 (2016).
8. Laliberté, F., Howell, S. & Kushner, P. Regional variability of a projected sea ice-free Arctic during the summer months. *Geophys. Res. Lett.* **43**, 256–263 (2016).
9. Hollowed, A. B., Planque, B. & Loeng, H. Potential movement of fish and shellfish stocks from the sub-Arctic to the Arctic Ocean. *Fish. Oceanogr.* **22**, 355–370 (2013).
10. Haug, T. et al. Future harvest of living resources in the Arctic Ocean north of the Nordic and Barents Seas: a review of possibilities and constraints. *Fish. Res.* **188**, 38–57 (2017).
11. Jung, T. et al. Advancing polar prediction capabilities on daily to seasonal time scales. *Bull. Am. Meteorol. Soc.* **97**, 1631–1647 (2016).
12. Francis, J. A. & Vavrus, S. J. Evidence linking Arctic amplification to extreme weather in mid-latitudes. *Geophys. Res. Lett.* **39**, L06801 (2012).
13. Cohen, J. et al. Recent Arctic amplification and extreme mid-latitude weather. *Nat. Geosci.* **7**, 627–637 (2014).
14. Coumou, D., Di Capua, G., Vavrus, S., Wang, L. & Wang, S. The influence of Arctic amplification on mid-latitude summer circulation. *Nat. Commun.* **9**, 1–12 (2018).
15. Cohen, J., Pfeiffer, K. & Francis, J. A. Warm Arctic episodes linked with increased frequency of extreme winter weather in the united states. *Nat. Commun.* **9**, 1–12 (2018).
16. Barnes, E. A. Revisiting the evidence linking Arctic amplification to extreme weather in midlatitudes. *Geophys. Res. Lett.* **40**, 4734–4739 (2013).
17. Kretschmer, M., Coumou, D., Donges, J. F. & Runge, J. Using causal effect networks to analyze different Arctic drivers of midlatitude winter circulation. *J. Clim.* **29**, 4069–4081 (2016).
18. Cohen, J. et al. Divergent consensuses on Arctic amplification influence on midlatitude severe winter weather. *Nat. Clim. Change* **10**, 20–29 (2020).
19. Blackport, R. & Screen, J. A. Weakened evidence for mid-latitude impacts of Arctic warming. *Nat. Clim. Change* **10**, 1065–1066 (2020).
20. Levine, X. J., Cvijanovic, I., Ortega, P., Donat, M. G. & Tourigny, E. Atmospheric feedback explains disparate climate response to regional Arctic sea-ice loss. *npj Clim. Atmos. Sci.* **4**, 1–8 (2021).
21. Liang, Y.-C. et al. Impacts of Arctic sea ice on cold season atmospheric variability and trends estimated from observations and a multimodel large ensemble. *J. Clim.* **34**, 8419–8443 (2021).
22. Pithan, F. & Mauritsen, T. Arctic amplification dominated by temperature feedbacks in contemporary climate models. *Nat. Geosci.* **7**, 181–184 (2014).
23. Huang, Y., Tan, X. & Xia, Y. Inhomogeneous radiative forcing of homogeneous greenhouse gases. *J. Geophys. Res.: Atmos.* **121**, 2780–2789 (2016).
24. Bintanja, R., Graversen, R. & Hazeleger, W. Arctic winter warming amplified by the thermal inversion and consequent low infrared cooling to space. *Nat. Geosci.* **4**, 758–761 (2011).
25. Taylor, P. C. et al. A decomposition of feedback contributions to polar warming amplification. *J. Clim.* **26**, 7023–7043 (2013).
26. Block, K. & Mauritsen, T. Forcing and feedback in the MPI-ESM-LR coupled model under abruptly quadrupled CO_2. *J. Adv. Model. Earth Sys.* **5**, 676–691 (2013).
27. Goosse, H. et al. Quantifying climate feedbacks in polar regions. *Nat. Commun.* **9**, 1–13 (2018).
28. Stuecker, M. F. et al. Polar amplification dominated by local forcing and feedbacks. *Nat. Clim. Change* **8**, 1076–1081 (2018).
29. Hwang, Y.-T., Frierson, D. M. & Kay, J. E. Coupling between Arctic feedbacks and changes in poleward energy transport. *Geophys. Res. Lett.* **38**, L17704 (2011).
30. Kay, J. E. et al. The influence of local feedbacks and northward heat transport on the equilibrium Arctic climate response to increased greenhouse gas forcing. *J. Clim.* **25**, 5433–5450 (2012).
31. Graversen, R. G. & Burtu, M. Arctic amplification enhanced by latent energy transport of atmospheric planetary waves. *Quart. J. Royal Meteorol. Soc.* **142**, 2046–2054 (2016).
32. Yoshimori, M., Abe-Ouchi, A. & Laîné, A. The role of atmospheric heat transport and regional feedbacks in the Arctic warming at equilibrium. *Clim. Dyn.* **49**, 3457–3472 (2017).
33. Graversen, R. G. & Langen, P. L. On the role of the atmospheric energy transport in $2 \times CO_2$-induced polar amplification in CESM1. *J. Clim.* **32**, 3941–3956 (2019).
34. Beer, E., Eisenman, I. & Wagner, T. J. Polar amplification due to enhanced heat flux across the halocline. *Geophys. Res. Lett.* **47**, e2019GL086706 (2020).
35. Chung, E.-S. et al. Cold-season Arctic amplification driven by Arctic ocean-mediated seasonal energy transfer. *Earth's Future* **9**, e2020EF001898 (2021).
36. Hankel, C. & Tziperman, E. The role of atmospheric feedbacks in abrupt winter Arctic sea ice loss in future warming scenarios. *J. Clim.* **34**, 4435–4447 (2021).
37. Feldl, N., Anderson, B. T. & Bordoni, S. Atmospheric eddies mediate lapse rate feedback and Arctic amplification. *J. Clim.* **30**, 9213–9224 (2017).
38. Feldl, N., Po-Chedley, S., Singh, H. K., Hay, S. & Kushner, P. J. Sea ice and atmospheric circulation shape the high-latitude lapse rate feedback. *npj Clim. Atmos. Sci.* **3**, 1–9 (2020).
39. Boeke, R. C. & Taylor, P. C. Seasonal energy exchange in sea ice retreat regions contributes to differences in projected Arctic warming. *Nat. Commun.* **9**, 1–14 (2018).
40. Boeke, R. C., Taylor, P. C. & Sejas, S. A. On the nature of the Arctic's positive lapse-rate feedback. *Geophys. Res. Lett.* **48**, e2020GL091109 (2020).
41. Screen, J. A. & Simmonds, I. The central role of diminishing sea ice in recent Arctic temperature amplification. *Nature* **464**, 1334–1337 (2010).
42. Bintanja, R. & Van der Linden, E. The changing seasonal climate in the Arctic. *Sci. Rep.* **3**, 1–8 (2013).
43. Bintanja, R. & Selten, F. Future increases in Arctic precipitation linked to local evaporation and sea-ice retreat. *Nature* **509**, 479–482 (2014).
44. Blackport, R. & Kushner, P. J. The transient and equilibrium climate response to rapid summertime sea ice loss in CCSM4. *J. Clim.* **29**, 401–417 (2016).
45. Oudar, T. et al. Respective roles of direct GHG radiative forcing and induced Arctic sea ice loss on the Northern Hemisphere atmospheric circulation. *Clim. Dyn.* **49**, 3693–3713 (2017).
46. McCusker, K. E. et al. Remarkable separability of circulation response to Arctic sea ice loss and greenhouse gas forcing. *Geophys. Res. Lett.* **44**, 7955–7964 (2017).
47. Blackport, R. & Kushner, P. J. Isolating the atmospheric circulation response to Arctic sea ice loss in the coupled climate system. *J. Clim.* **30**, 2163–2185 (2017).
48. Smith, D. M. et al. Atmospheric response to Arctic and Antarctic sea ice: the importance of ocean–atmosphere coupling and the background state. *J. Clim.* **30**, 4547–4565 (2017).
49. Taylor, P. C., Hegyi, B. M., Boeke, R. C. & Boisvert, L. N. On the increasing importance of air-sea exchanges in a thawing Arctic: a review. *Atmosphere* **9**, 41 (2018).

50. Dai, A., Luo, D., Song, M. & Liu, J. Arctic amplification is caused by sea-ice loss under increasing CO_2. *Nat. Commun.* **10**, 1–13 (2019).

51. Kim, K.-Y. et al. Vertical feedback mechanism of winter Arctic amplification and sea ice loss. *Sci. Rep.* **9**, 1–10 (2019).

52. Screen, J. A. & Simmonds, I. Increasing fall-winter energy loss from the Arctic Ocean and its role in Arctic temperature amplification. *Geophys. Res. Lett.* **37**, L16707 (2010).

53. Laîné, A., Yoshimori, M. & Abe-Ouchi, A. Surface Arctic amplification factors in CMIP5 models: land and oceanic surfaces and seasonality. *J. Clim.* **29**, 3297–3316 (2016).

54. Burt, M. A., Randall, D. A. & Branson, M. D. Dark warming. *J. Clim.* **29**, 705–719 (2016).

55. Deser, C., Tomas, R., Alexander, M. & Lawrence, D. The seasonal atmospheric response to projected Arctic sea ice loss in the late twenty-first century. *J. Clim.* **23**, 333–351 (2010).

56. Graversen, R. G., Langen, P. L. & Mauritsen, T. Polar amplification in CCSM4: contributions from the lapse rate and surface albedo feedbacks. *J. Clim.* **27**, 4433–4450 (2014).

57. Deser, C., Tomas, R. A. & Sun, L. The role of ocean–atmosphere coupling in the zonal-mean atmospheric response to Arctic sea ice loss. *J. Clim.* **28**, 2168–2186 (2015).

58. Jenkins, M. & Dai, A. The impact of sea-ice loss on Arctic climate feedbacks and their role for Arctic amplification. *Geophys. Res. Lett.* **48**, e2021GL094599 (2021).

59. Lebrun, M., Vancoppenolle, M., Madec, G. & Massonnet, F. Arctic sea-ice-free season projected to extend into autumn. *Cryosphere* **13**, 79–96 (2019).

60. Årthun, M., Onarheim, I. H., Dörr, J. & Eldevik, T. The seasonal and regional transition to an ice-free Arctic. *Geophys. Res. Lett.* **48**, e2020GL090825 (2021).

61. Holland, M. M. & Landrum, L. The emergence and transient nature of Arctic amplification in coupled climate models. *Front. Earth Sci.* **9**, 764 (2021).

62. Holland, M. M. & Bitz, C. M. Polar amplification of climate change in coupled models. *Clim. Dyn.* **21**, 221–232 (2003).

63. Ding, Q. et al. Fingerprints of internal drivers of Arctic sea ice loss in observations and model simulations. *Nat. Geosci.* **12**, 28–33 (2019).

64. England, M., Jahn, A. & Polvani, L. Nonuniform contribution of internal variability to recent Arctic sea ice loss. *J. Clim.* **32**, 4039–4053 (2019).

65. Landrum, L. & Holland, M. M. Extremes become routine in an emerging new Arctic. *Nat. Clim. Change* **10**, 1108–1115 (2020).

66. England, M., Eisenman, I., Lutsko, N. & Wagner, T. J. W. The recent emergence of Arctic amplification. *Geophys. Res. Lett.* **48**, e2021GL094086 (2021).

67. Meinshausen, M. et al. The shared socio-economic pathway (SSP) greenhouse gas concentrations and their extensions to 2500. *Geosci. Model Dev.* **13**, 3571–3605 (2020).

68. Mitevski, I., Orbe, C., Chemke, R., Nazarenko, L. & Polvani, L. M. Non-monotonic response of the climate system to abrupt CO_2 forcing. *Geophys. Res. Lett.* **48**, e2020GL090861 (2021).

69. Deser, C., Sun, L., Tomas, R. A. & Screen, J. Does ocean coupling matter for the northern extratropical response to projected Arctic sea ice loss? *Geophys. Res. Lett.* **43**, 2149–2157 (2016).

70. Tomas, R. A., Deser, C. & Sun, L. The role of ocean heat transport in the global climate response to projected Arctic sea ice loss. *J. Clim.* **29**, 6841–6859 (2016).

71. He, S., Xu, X., Furevik, T. & Gao, Y. Eurasian cooling linked to the vertical distribution of Arctic warming. *Geophys. Res. Lett.* **47**, e2020GL087212 (2020).

72. Labe, Z., Peings, Y. & Magnusdottir, G. Warm Arctic, cold Siberia pattern: role of full Arctic amplification versus sea ice loss alone. *Geophys. Res. Lett.* **47**, e2020GL088583 (2020).

73. Kim, D., Kang, S. M., Merlis, T. M. & Shin, Y. Atmospheric circulation sensitivity to changes in the vertical structure of polar warming. *Geophys. Res. Lett.* **48**, e2021GL094726.

74. Deser, C. et al. Insights from earth system model initial-condition large ensembles and future prospects. *Nat. Clim. Change* **10**, 277–286 (2020).

75. Kay, J. E. et al. The Community Earth System Model (CESM) large ensemble project: a community resource for studying climate change in the presence of internal climate variability. *Bull. Am. Meteorol. Soc.* **96**, 1333–1349 (2015).

76. Bonan, D. B., Lehner, F. & Holland, M. M. Partitioning uncertainty in projections of Arctic sea ice. *Environ. Res. Lett.* **16**, 044002 (2021).

77. Lehner, F. et al. Partitioning climate projection uncertainty with multiple large ensembles and CMIP5/6. *Earth System Dyn.* **11**, 491–508 (2020).

78. Cai, Z. et al. Arctic warming revealed by multiple CMIP6 models: evaluation of historical simulations and quantification of future projection uncertainties. *J. Clim.* **34**, 4871–4892 (2021).

79. Hahn, L. C., Armour, K. C., Zelinka, M. D., Bitz, C. M. & Donohoe, A. Contributions to polar amplification in CMIP5 and CMIP6 models. *Front. Earth Sci.* **9**, 1–17 (2021).

80. Hahn, L. C., Armour, K. C., Battisti, D. S., Eisenman, I. & Bitz, C. M. Seasonality in Arctic warming driven by sea ice effective heat capacity. *J. Clim.* 1–44 (2021).

81. Henry, M., Merlis, T. M., Lutsko, N. J. & Rose, B. E. Decomposing the drivers of polar amplification with a single-column model. *J. Clim.* **34**, 2355–2365 (2021).

82. Bitz, C. M. et al. Climate sensitivity of the community climate system model, version 4. *J. Clim.* **25**, 3053–3070 (2012).

83. Kirchmeier-Young, M. C., Zwiers, F. W. & Gillett, N. P. Attribution of extreme events in Arctic sea ice extent. *J. Clim.* **30**, 553–571 (2017).

84. Jeffrey, S. et al. Australia's CMIP5 submission using the CSIRO-Mk3.6 model. *Aust. Meteor. Oceanogr. J.* **63**, 1–14 (2013).

85. Sun, L., Alexander, M. & Deser, C. Evolution of the global coupled climate response to Arctic sea ice loss during 1990–2090 and its contribution to climate change. *J. Clim.* **31**, 7823–7843 (2018).

86. Rodgers, K. B., Lin, J. & Frölicher, T. L. Emergence of multiple ocean ecosystem drivers in a large ensemble suite with an earth system model. *Biogeosciences* **12**, 3301–3320 (2015).

87. Maher, N. et al. The Max Planck Institute Grand Ensemble: enabling the exploration of climate system variability. *J. Adv. Model. Earth Syst.* **11**, 2050–2069 (2019).

88. Eyring, V. et al. Overview of the Coupled Model Intercomparison Project Phase 6 (cmip6) experimental design and organization. *Geosci. Model Develop.* **9**, 1937–1958 (2016).

AUTHOR CONTRIBUTIONS

Y.-C.L. performed the analyses, and I.M. carried out the abrupt CO_2 forcing model experiments with CESM1. All authors interpreted and discussed the results. Y.-C.L. drafted the manuscript, and L.M.P. and I.M. were involved critical revisions. All authors approved the final manuscript.

COMPETING INTERESTS

The authors declare no competing interests.

ADDITIONAL INFORMATION

Supplementary information The online version contains supplementary material available at https://doi.org/10.1038/s41612-022-00228-8.

Correspondence and requests for materials should be addressed to Yu-Chiao Liang.

Reprints and permission information is available at http://www.nature.com/reprints

Publisher's note Springer Nature remains neutral with regard to jurisdictional claims in published maps and institutional affiliations.